Journal of Geophysical Research: Space Physics

RESEARCH ARTICLE
10.1029/2018JA025490

Key Points:
- Timing analysis of Chandra observations of Jupiter's X-ray auroras from 1999 to 2015
- Statistically significant quasi-periodicities in jovian auroral X-rays are relatively rare and periods variable, even on successive planetary rotations
- We use Rayleigh testing and Monte Carlo simulation to search for statistically significant quasi-periods in sparse, time-tagged data

Supporting Information:
- Supporting Information S1
- Data Set S1
- Data Set S2
- Data Set S3
- Data Set S4
- Figure S1

Correspondence to:
C. M. Jackman,
c.jackman@soton.ac.uk

Citation:
Jackman, C. M., Knigge, C., Altamirano, D., Gladstone, R., Dunn, W., Elsner, R., et al. (2018). Assessing quasi-periodicities in Jovian X-ray emissions: Techniques and heritage survey. *Journal of Geophysical Research: Space Physics, 123*, 9204–9221. https://doi.org/10.1029/2018JA025490

Received 19 MAR 2018
Accepted 1 OCT 2018
Accepted article online 6 OCT 2018
Published online 13 NOV 2018

Assessing Quasi-Periodicities in Jovian X-Ray Emissions: Techniques and Heritage Survey

C. M. Jackman[1], C. Knigge[1], D. Altamirano[1], R. Gladstone[2], W. Dunn[3,4,5], R. Elsner[6], R. Kraft[5], G. Branduardi-Raymont[3], and P. Ford[7]

[1]Department of Physics and Astronomy, University of Southampton, Southampton, UK, [2]Space Science and Engineering Division, Southwest Research Institute, San Antonio, TX, USA, [3]Mullard Space Science Laboratory, Department of Space and Climate Physics, University College London, London, UK, [4]The Centre for Planetary Science at UCL/Birkbeck, Gower Street, London, UK, [5]Harvard-Smithsonian Center for Astrophysics, Smithsonian Astrophysical Observatory, Cambridge, MA, USA, [6]NASA Marshall Space Flight Center, USA, [7]Kavli Institute for Astrophysics and Space Research, MIT, Cambridge, MA, USA

Abstract Jupiter's auroral X-rays are rather mysterious, with an unknown driver, and several previous reports of individual cases of quasi-periodic emission. In this work we revisit heritage X-ray data sets from the 1990s to 2015 and apply robust significance testing of emerging quasi-periodicities, seeking to understand the robustness and regularity of previously reported quasi-periodic emissions. Our analysis incorporates the use of the Rayleigh test as an alternative to Lomb-Scargle analysis or Fast Fourier Transforms, where Rayleigh is particularly suited to a time-tagged data set of sparse counts such as is common for jovian X-ray data. Furthermore, the analysis techniques that we present (including Rayleigh testing and Monte Carlo simulation) can be applied to any time-tagged data set. The code to conduct such analysis is released as supplementary information to accompany this paper. The five most significant (p value <0.01) quasi-periods from Jupiter's northern auroral region have periods ranging from ~8.0 to 45.96 min, and the two most significant (p value <0.01) quasi-periods from the south have periods of ~14.1 and ~34.9 min. The selection of a restrictive hot spot source region seems to be critical for detecting quasi-periodic emission, suggesting that the site of pulsations may be spatially localized. Periods vary from one Jupiter rotation to the next in one long observation, and the north and south are shown to pulse independently in another conjugate observation. These results have important implications for understanding the driver of jovian X-ray emission.

1. Introduction

Jupiter's X-ray emission was first discovered using data from the Einstein observatory (Metzger et al., 1983). In more recent years Jupiter's X-rays have been studied using the Chandra, XMM-Newton, and NuSTAR observatories. The X-ray emissions from the planet's disk and the auroral regions have been characterized separately, with the former found to be produced via elastic scattering and fluorescence of solar X-ray photons in the upper atmosphere (e.g., Bhardwaj et al., 2005; Maurellis et al., 2000) and the latter due to charge exchange interactions between precipitating ions and atmospheric neutral hydrogen molecules (e.g., Cravens et al., 1995; Cravens & Ozak, 2012) and bremsstrahlung from precipitating electrons (Branduardi-Raymont et al., 2004, 2007).

The auroral X-ray emissions themselves consist of two key components. The first is the main oval emission, produced when precipitating electrons emit bremsstrahlung which dominates the spectrum above 2 keV (Branduardi-Raymont et al., 2007, 2008). The second is the hot spot, generated when ions precipitating into the upper atmosphere produce soft X-ray lines through charge exchange collisions with atmospheric neutral hydrogen molecules (e.g., Cravens et al., 2003; Elsner et al., 2005). A northern polar region hot spot was first discovered by Chandra during the year 2000 Cassini flyby of Jupiter (Gladstone et al., 2002; hereafter G02), and XMM spectral analysis showed that the precipitating ions which cause the hot spot comprise mostly oxygen and carbon/sulfur (e.g., Branduardi-Raymont et al., 2007), albeit with an unknown source. More recently, Dunn et al. (2017; hereafter D17) reported the discovery of an independent southern auroral X-ray hot spot.

One of the interesting features of the auroral emissions, and the hot spots in particular, is that they have occasionally been observed to pulse quasi-periodically. G02 reported a 45-min quasi-periodic oscillation of a severely spatially restricted northern hot spot region observed on 18 December 2000. Such an oscillation has not been reported since, although examination of high energy electron bursts (McKibben et al., 1993)

and 10–20 kHz radio bursts (MacDowall et al., 1993) suggest that there may be something special about this ~45 min timescale in terms of Jupiter's magnetospheric dynamics. D17 also performed a strict spatial selection, in this case of the southern auroral region, and reported a quasi-periodic pulsing of the southern hot spot every ~11 min observed by both Chandra and XMM during an observation on 24 May 2016. Several campaigns were planned in 2011 to coincide with the expected arrival of a coronal mass ejection at Jupiter (in order to learn more about the influence of the solar wind on jovian X-rays), and the data from these campaigns were analyzed in Dunn et al. (2016) who reported an ~26-min quasi-period from sulfur ions, and an ~12-min period from a combination of carbon/sulfur and oxygen ions in the northern auroral region. Dunn et al. (2016) found that the periodic behavior was spatially localized and noted that other broader polar emissions did not feature the regularity. The results on the nature of solar wind driving have been somewhat mixed (e.g., Dunn et al., 2016; Kimura et al., 2016) due to the difficulty of relying on propagated solar wind parameters from models, as opposed to in situ measurements from an upstream monitor. Results suggest a possible relationship with the solar wind, but quite how the X-ray emissions relate to this remains uncertain. Data from the Juno approach campaigns in 2016 should help to shed more light on this relationship.

However, these are just a small handful of reported quasi-periods compared to the much larger catalogue of observations: ~24 Chandra observations in the pre-Juno era alone, plus ~12 (pre-Juno) with XMM and more recently with NuStar. Understanding periodicities (and their absence) is important as it may provide clues as to the unknown driver of Jupiter's auroral X-ray emission. One possible candidate for a driver of quasi-periodic X-ray emission is the pulsed reconnection process put forward by Bunce et al. (2004): they conclude that the timescale required for feedback between Jupiter's ionosphere and magnetosphere may be ~40 min (given the large distances for particles to travel), which matches the 45-min period reported by G02 well. Bonfond et al. (2011) invoked pulsed dayside reconnection and subsequent ion precipitation to explain quasi-periodic 2- to 3-min UV flares detected with HST in the jovian aurora (because of the 1- to 4-min reoccurrence time between consecutive Flux Transfer Event signatures observed at Jupiter's magnetopause by Walker & Russell, 1985). Subsequently, Bonfond et al. (2016) revisited the puzzle of 2- to 3-min period UV flares, suggesting that they may instead take place on closed field lines in the outer magnetosphere. The flaring behavior was observed to be rather restricted to a limited portion of the polar region and to appear for only a fraction (approximately half) of a typical 45-min HST observation sequence. Most recently, Nichols et al. (2017) examined further HST UV observations of the jovian aurora and reported a pulsating emission within Jupiter's main auroral oval, with period ~10 min, which they claim is similar to the expected Alfvén travel time between the ionosphere and the upper edge of the equatorial plasma sheet in the middle magnetosphere. There are two key caveats to bear in mind when comparing reported quasi-periods from X-ray and UV observations: (i) the emissions in the two wavelengths differ in that the X-ray emission is related to upward-going electrons (downward-going ions), and the UV emission is related to downward-going electrons, and thus the source/driver may be different, (ii) the HST observation window is ~45 min and thus only really suitable for searching for relatively short (~15 min or shorter) UV periods. On the other hand, the X-ray observation windows with Chandra and XMM are much longer and thus better suited to the search for longer timescale quasi-periods, albeit with lower photon counts.

In this paper we conduct a thorough and complete survey of all Chandra observation campaigns from 1999 to 2015 (pre-Juno era) to systematically search the auroral X-ray data for evidence of quasi-periodicities and to examine the statistical significance of any emerging quasi-periods. In section 2 we outline the details of the data set and any preprocessing. Section 3 outlines our analysis methods and shows results from timing analysis, including a Monte Carlo simulation for calculating statistical significance. Section 4 places the results in a statistical context, comparing all previous observation campaigns. We highlight the advantages of the timing analysis methods that we have employed, as well as cautioning against possible pitfalls in timing analysis, and limitations of the available data sets. Section 5 summarizes the results and looks to the future of Juno era exploration of Jupiter from a joint in situ remote sensing perspective.

2. Data Sets

The Chandra X-ray Observatory conducted observations of Jupiter 24 times between 1999 and 2015, and the dates of the 20 observations with recoverable data suitable for our purpose are illustrated in Figure 1 versus sunspot number. It is evident that observations have taken place across various stages of the solar cycle from

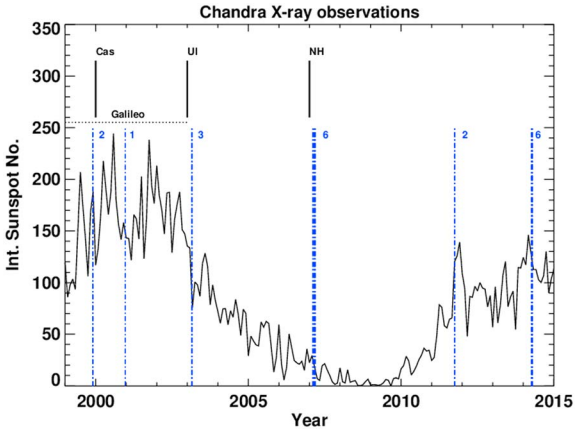

Figure 1. Sunspot number as a function of time from 1999 to 2015. The times of X-ray observations with Chandra are marked by vertical dot-dashed blue lines. Blue labels to the right of vertical lines show the number of individual Chandra observations in a given campaign interval. The times of spacecraft flybys of Jupiter (with concurrent in situ solar wind and/or magnetospheric data) are shown by the vertical black lines for Cas, UI, and NH. The interval of the orbital mission Galileo is marked by the horizontal black dotted line. CAS = Cassini; UI = Ulysses; NH = New Horizons.

minimum to maximum, clustered to coincide with in situ spacecraft measurement of the upstream solar wind and/or the planetary magnetosphere. The observations in 2011 and 2014 were both planned to coincide with the expected arrival of a coronal mass ejection, to explore the response of Jupiter's X-rays to strong solar wind driving. The specific times, dates, observation durations, and Chandra ObsIDs are listed in Table 1.

Chandra X-ray Observatory has two on-board cameras which have been used to image Jupiter: the High-Resolution Camera (HRC-I) and the Advanced CCD Imaging Spectrometer (ACIS). The raw data first have to be transformed into a frame of reference centered on Jupiter using appropriate ephemerides data from the JPL HORIZONS program and Chandra orbit ancillary data provided with the Chandra X-ray Center data product packages. We did not conduct any background subtraction as the planet blocks X-rays emitted from distant sources, and the particle background suppression by the instruments themselves is good (background rates of 0.00088 and 0.014 counts per second off the planet from ACIS and HRC, respectively; see, e.g., Elsner et al., 2005).

Once the data are reregistered on Jupiter (in our case using the CIAO *sso_freeze* program; Fruscione et al., 2006) it is possible to conduct manual region selection to highlight the northern and southern auroral regions (noting that photons which are observed closest to the planet's limb are subject to the largest uncertainties in terms of mapping). The auroral photons are much more concentrated than the background or planetary disk photons and thus are relatively easy to manually select. We then wish to select a subset of these auroral regions which correspond to the hot spot emission. The northern hot spot

Table 1
List of Chandra Observations of Jupiter's X-Rays From 1999 to 2015 (all pre-Juno era)

Telescope-instrument-region	Start date (year-month-day hr:min:s)	Dur. of obs. (ks)	Obs ID
Chandra-ACIS-S	1999-11-25 07:59:41	20	1
Chandra-ACIS-S	1999-11-25 13:52:54	20	1482
Chandra-ACIS-S	1999-11-25 19:26:54	22	960
Chandra-ACIS-S	1999-11-26 01:58:53	22	1463
Chandra-ACIS-S	1999-11-26 14:23:54	14	1464
Chandra-ACIS-S	1999-11-26 19:55:53	23	1465
Chandra-HRC-I	2000-12-18 09:53:23	36	1862
Chandra-ACIS-S	2003-02-24 15:36:22	30	3726
Chandra-HRC-I	2003-02-25 00:21:20	72	2519
Chandra-ACIS-S	2003-02-25 20:16:52	41	4418
Chandra-ACIS-S	2007-02-08 08:29:44	18	7405
Chandra-ACIS-S	2007-02-10 19:53:21	18	8216
Chandra-ACIS-S	2007-02-24 21:23:16	18	8217
Chandra-ACIS-S	2007-03-03 07:41:28	18	8219
Chandra-ACIS-S	2007-03-07 14:17:52	18	8220
Chandra-ACIS-S	2007-03-08 21:02:26	18	8218
Chandra-ACIS-S	2011-10-02 21:54:26	40	12315
Chandra-ACIS-S	2011-10-04 14:33:08	40	12316
Chandra-HRC-I	2014-04-08 08:18:10	40	15671
Chandra-HRC-I	2014-04-10 01:09:23	40	16299
Chandra-HRC-I	2014-04-12 22:09:30	40	15672
Chandra-HRC-I	2014-04-15 20:43:04	40	15669
Chandra-HRC-I	2014-04-17 12:19:31	40	16300
Chandra-HRC-I	2014-04-20 02:19:30	40	15670

Note. The first four observations in 1999 (1, 1482, 960, 1463) suffered an on-board problem which means the data are not recoverable for the purposes of disk or auroral imaging (P. Ford, personal communication, 2018). The columns give the observation instrument, observation start date, the duration of the entire observation in kilosecond, and the Observation ID from the Chandra archive (which does not always follow chronological order). ACIS = Advanced CCD Imaging Spectrometer; HRC = High-Resolution Camera.

has been found in previous work to be fixed between longitudes of 155–190°, while the southern hot spot is fixed at longitudes of 0–75° (as we will see later results are highly sensitive to this selection). In order to select the time interval between the hot spot longitude entering into view and exiting view, we select times from System III CML 155–90° (65°) to CML 190 + 90° (280°) for the north, and corresponding values for the south (using the NASA JPL HORIZONS program). This method does not place any constraints on latitude, and thus while we expect the portion of Jupiter observed during this longitude visibility window to be dominated by hot spot photons, it may also include some non-hot spot emission.

3. Results

In this section we show an example of Chandra light curve timing analysis, along with techniques to conduct significance testing of periods.

3.1. Rayleigh Testing

A review of the literature indicates that the vast majority of published timing analyses of planetary auroral emissions (X-rays, UV) involve the application of Lomb-Scargle analysis (Horne & Baliunas, 1986; Lomb, 1976; Scargle, 1982). Lomb-Scargle analysis is a specific method of spectral analysis, initially developed for use with unevenly sampled data, based on evaluating sines and cosines only at times t_i that are actually measured. The analysis then returns a Lomb-Scargle normalized periodogram which gives spectral power as a function of angular frequency ($\omega = 2\pi f$).

The statistical significance of Lomb-Scargle power P_{LS} associated with a putative periodic signal is then commonly evaluated via the so-called *False Alarm Probability*, FAP_1. FAP_1 is the *p* value associated with the null hypothesis that a spectral power as high as P_{LS} should be produced by Gaussian white noise with the same variance as found in the actual data. However, there are at least three significant problems associated with the application of Lomb-Scargle analysis in practice, especially in the context of X-ray data.

First, FAP_1 is a *single-trial* *p* value associated with one, randomly selected frequency. By contrast, in practice, one typically inspects a wide and finely sampled frequency grid and then selects the frequency associated with the highest peak in the power spectrum (P_{LS_MAX}) as the frequency of the putative periodic signal. Unsurprisingly, the probability of finding a maximum power as high as P_{LS_MAX} is not given by FAP_1 and is typically much higher. This is sometimes referred to as the *look-elsewhere effect*. In principle, this can be overcome by using the multiple-trial *p* value, FAP_M. This is the probability that pure Gaussian white noise will produce a spectral power as high as P_{LS} at least once in M independent trials. Unfortunately, the very concept of *independent frequencies* is ill-defined for unevenly spaced data. A conservative approach is to set M to the total number of frequencies that were searched, but this can seriously diminish the statistical power of the analysis. A much better approach is to estimate the appropriate multitrial false alarm probability directly from numerical simulations.

Second, real-life data sets often contain red noise. This term describes aperiodic stochastic variability in which any two data points exhibit correlations whose strength is a function of the time interval that separates them. Red noise is distinct from white noise which produces globally flat power spectra. Statistical tests such as Lomb-Scargle based on a white noise (e.g., Gaussian) null hypothesis will tend to overestimate the actual significance of a putative periodic signal when applied to data containing red noise—sometimes dramatically so.

Third, many time series—especially in X-ray astronomy—do not consist of a continuous signal sampled at specific times, but instead represent individual time-tagged *events* (e.g., photon counts). In order to apply techniques like Lomb-Scargle analysis to such data sets, it is necessary to bin the observations, thus immediately reducing the range of frequencies that can be investigated. Moreover, if the entire data set contains relatively few counts (like the jovian X-ray data in this study), the rebinned version will likely display Poisson, rather than Gaussian statistics.

In this work, we attempt to overcome these problems. We deal with the look-elsewhere effect by carrying out extensive Monte Carlo simulations. We test for the presence of red noise by checking if our power spectra show the characteristic linear decline with frequency in log-log space. Finally, we account for the sparse and event-based nature of our X-ray data sets by using power spectra based on the Rayleigh statistic (Leahy et al., 1983; Mardia, 1972). Rayleigh is one of a family of statistical tests (see also the Z_m^2 test,

Buccheri et al., 1983, and the H-test, DeJager et al., 1989) which all work on unbinned, time-tagged data (e.g., X-ray photon arrival times). All of these tests construct a phase diagram for the photon arrival times and test this against uniformity. In the Rayleigh test, the test statistic is designed to be maximally sensitive to a sinusoidal signal. The Rayleigh test associates each time-tagged photon with a phase for each assumed frequency and then looks to see whether the distribution of phases is uniform, or whether there are any local anomalies. The test statistic maximizes the difference between the null hypothesis of *no signal* against the alternative hypothesis of a periodic signal. A uniform distribution is taken to indicate the absence of a period in a given time series, whereas an anomalous distribution (with a preference for particular phases) implies there may be a significant period present. The Rayleigh Power, R_P, is defined as

$$R_p = \frac{(\sum \cos\omega t)^2 + (\sum \sin\omega t)^2}{N}, \quad (1)$$

where ω is a set of angular frequencies to test against (chosen to span a range commensurate with the timescale of the observation and cadence of data). Here t is the array containing the times of arrival of individual photons, with N the total number of photon counts over the observation interval. Data containing a signal (colored noise, quasi-periodic, and strictly periodic) at some frequency will produce a high Rayleigh power at that frequency.

One of the primary advantages of using the Rayleigh statistic for data sets such as jovian X-rays is that it is run on unbinned, unsmoothed data, thus avoiding disadvantages due to binning (e.g., Gibson et al., 1982). These disadvantages include (i) losing information on timescales shorter than the binsize and (ii) introducing bias due to somewhat arbitrary bin selection. Whenever binning is employed, information is lost, and this is particularly undesirable in such a low count regime as the jovian X-ray data sets under examination here. The statistical power of the Rayleigh statistic is highest for *smooth* quasi-sinusoidal periodic signals. More complex signals, such as sharp pulses, produce a lot of power at the higher order harmonics associated with their fundamental frequency. Extensions of the basic Rayleigh statistic such as the Z_m^2 test, the H-test, or the modified Rayleigh statistic are designed to be more powerful for detecting such signals (e.g., Bélanger, 2016). Rayleigh testing has been used widely in the X-ray and γ-ray astronomy communities (e.g., Brazier, 1994) and holds immense promise for use in planetary science on the wealth of multiwavelength planetary auroral time-tagged data sets. It is straightforward to implement, and in order to facilitate community engagement with this method, we provide code in both IDL and Python in this paper's supporting information so that the test can be applied to users' own data sets. In the sections below we describe the use of the Rayleigh statistic to search for quasi-periods in jovian X-ray data. Confidence/statistical significance levels are extracted from the Rayleigh analysis results by running thousands of Monte Carlo simulations as detailed in section 3.2 below.

3.2. Monte Carlo Simulations and Number of Trials

When applying Rayleigh analysis to X-ray data to search for (quasi)-periods, we want to estimate the likelihood of observing a maximum peak as high as observed in our data, under the null hypothesis that there is no signal. As such we conduct Monte Carlo simulations. We start with the initial light curve with no binning or smoothing: a simple list of arrival times of time-tagged photons. We record the total number of X-ray photons in the observation window and then use a random number generator to randomly distribute these photons across the time window in order to destroy any correlations or inherent periodicities. Thus, the shuffled *fake* data set has the same number of photons over the same total time as the real input data, but the photon arrival times are completely randomized. We then run the exact same analysis that we use on the real data—using the exact same frequency grid—for 10,000 different shuffled combinations. For each mock data set, we store the maximum power found across all search frequencies and compare the histogram of these maximum powers against the maximum peak power obtained from the Rayleigh analysis of the input data. In this way we can calculate a significance from the Monte Carlo simulations: for example, if 1 out of 10,000 trials on fake shuffled data returned a power higher than the peak power from the real data, we would quote a significance level (i.e., (1-p) $\times$ 100) of 99.99% (p value of 0.0001). Since we analyze each data set in exactly the same way as the real data—which includes scanning the same frequency grid for the maximum peak power—this significance takes the look-elsewhere effect associated with searching multiple frequencies fully into account. More specifically, the null hypothesis associated with our p value is that a maximum power as high as observed should be found *at any of our search frequencies* if the observed

events are randomly distributed throughout the observing interval. The search grid that we use for the analyses in this paper contains 1,500 equally linearly spaced frequencies corresponding to the period range between 2 and 100 min. This period search ensures that we avoid undersampling (ensuring that each peak in the power spectrum is fully resolved) and that we fully explore the expected domain given the cadence of the data and the duration of observation intervals.

As described above, our Monte Carlo simulations account for the fact that we inspect many frequencies when searching for a periodic signal. However, there are other types of look-elsewhere effect that the simulations do not deal with. For example, since periodic signals that have so far been claimed span a range of frequencies and have only been seen in a small subset of all observations (e.g., G02 45 min northern hot spot, D17 11 min southern hot spot), we search several independent data sets individually for the presence of such signals.

Overall, it seems clear that there is a significant knowledge gap in terms of the driver of the emission, and hence any expected period. Our lack of understanding of the physics that produces Jupiter's X-rays (periodic or otherwise) means that we do not know whether different observations of Jupiter can be considered to occur under vastly different driving conditions or not. We are uncertain about the driver of the potential signals we report, and furthermore we expect to have a low number of observations which were conducted under any given circumstance (e.g., upstream solar wind conditions, magnetospheric state, jovian season). In order to account for multiple trials of this type, we note that, in N independent searches that each adopt a critical p value of p, one should expect to find $N*p$ false positives. We therefore deal with this by adopting sufficiently conservative critical p values (while still showing the full range of p values in Figure 3 below for completeness).

3.3. Light Curve Timing Analysis

The X-ray data from the Chandra HRC and ACIS instruments come in the form of time-tagged photons from Jupiter. As explained in section 2 above, we take these raw data, process to account for Jupiter's motion, select the northern and southern auroral zones, and then further separate times when the hot spot regions are visible. Figure 2 shows analysis of a set of data taken by the Chandra HRC-I instrument. This particular observation campaign began on 25 February 2003 at 00:21 and lasted for 72 ks, allowing for examination of two consecutive Jupiter rotations, and hence exploration of any rotation-to-rotation variability in the X-ray emission. We note that there were further Chandra ACIS observations bracketing this 72 ks interval (ObsIDs 3726 and 4418), as analyzed in detail by Elsner et al. (2005), with our results from these shown in Table 2. The interval shown in Figure 2 spans from 02:05 to 07:55 on 25 February and represents the first of two intervals during the HRC observation when the northern hot spot region (see section 2 for definition) was visible. In the 5 hr 40 min interval shown here, 303 X-ray photons were registered by the Chandra HRC detector.

Figure 2a shows the light curve, with X-ray photons from the northern hot spot region binned into 60-s bins. The quantized nature of the emission is evident, with many time bins containing no photons at all. It is important to emphasize that these 0 values are true nondetections and thus contain information (as opposed to representing data gaps). Indeed, even for this time interval, which includes the hot spot (the most intense region of jovian X-ray emission), 147 out of 344 60-s time bins have 0 photon counts. The 125 bins have 1 count, 48 bins have 2 counts, 16 bins have 3 counts, 6 bins have 4 counts, and 2 bins have 5 counts.

Figures 2b and 2c give the results of Rayleigh analysis, with Figure 2b showing power versus period. The peak power of ~16.6 is marked by the vertical dot-dashed blue line, corresponding to a quasi-period of ~33.1 min. In order to visually inspect the data for red noise characteristics, Figure 2c shows the same results from the Rayleigh analysis plotted on a log (Power) versus log (Frequency) scale. The distribution in Figure 2c is reasonably flat, without strong evidence of a nonzero power law slope (we note that such a slope emerges if the data are smoothed, and we discuss the impact of smoothing further in section 4 below). Assessing how red noise may impact the sensitivity of our calculated significances is outside the scope of this work, but we refer the reader to Vaughan (2005) for detailed methods of significance testing (on plentiful input data counts) given red noise data.

We want to estimate the likelihood of observing a given peak if the null hypothesis (no periodicity in input data set) is true. We thus conduct Monte Carlo analysis as outlined in section 3.2 above, and show the histogram of the results in Figure 2d. We shuffled the initial light curve from Figure 2a 10,000 times, ran the

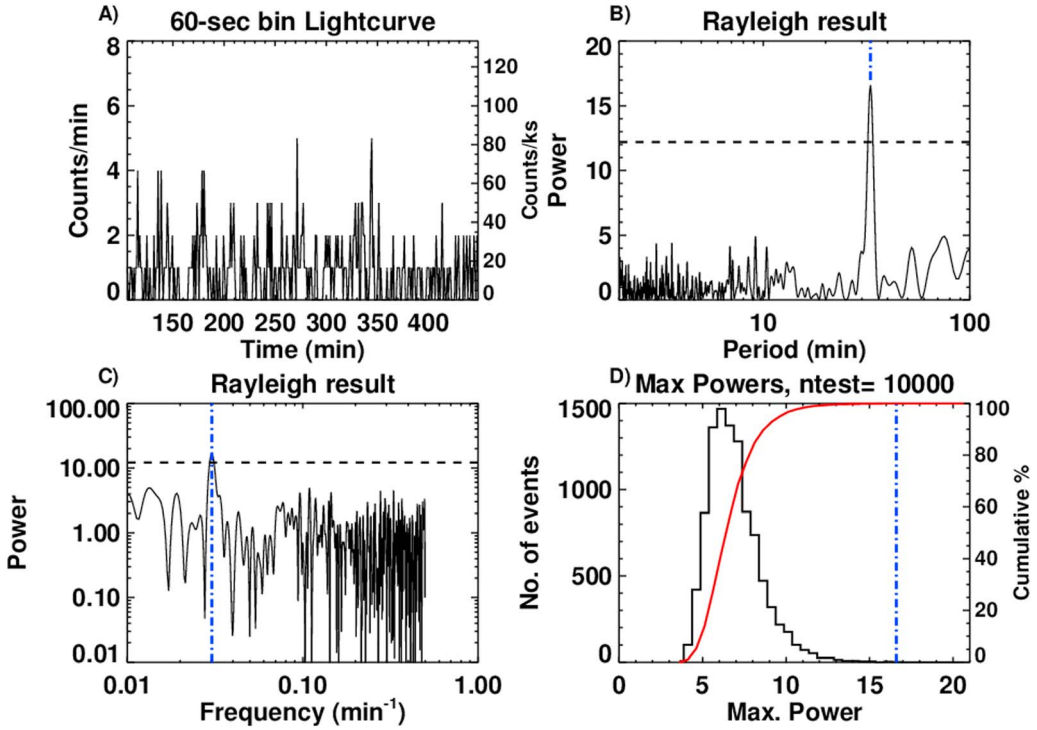

Figure 2. Light curve and timing analysis of X-ray photons from Jupiter's northern auroral hot spot measured by Chandra on 25 February 2003 during a subset of ObsID#2519. (a) Light curve of time-tagged photons binned into 60-s bins (unsmoothed), (b) power (arbitrary units) versus period from the Rayleigh test on input light curve. Peak power (associated with *best* quasi-period of ~33.1 min) marked by vertical dot-dashed blue line. Power associated with 99th percentile of 10,000 Monte Carlo simulations marked by horizontal black dashed line. (c) Power versus frequency from the Rayleigh test plotted on a log-log scale to test for the power law signature associated with red noise. Extended vertical dot-dashed blue line in the same format as panel (b). (d) Histogram of maximum powers from Rayleigh analysis of 10,000 randomly shuffled light curves based on original data. Peak power (associated with best quasi-period of original raw data) marked by vertical dot-dashed blue line. The red line shows the cumulative probability distribution of the maximum powers.

Rayleigh test, and the histogram of the maximum powers from these 10,000 runs is shown in Figure 2d. As in Figures 2b and 2c, the vertical dot-dashed blue line shows the power of the highest peak from the analysis of the raw (real) unbinned data. This peak lies firmly in the tail of the distribution, with only 6 out of 10,000 pure-noise mock data sets producing a maximum peak power greater than the value of 16 produced by the real data. As such we claim that the highest power peak from the Rayleigh analysis of the real data (power 16.6 at quasi-period of ~33.1 min) lies at the 99.94% significance level (p value 0.0006). We also extract the 99th percentile power from the Monte Carlo analysis. If we convert Figure 2d into a cumulative distribution as shown by the red line, we find that 99% (9,900 out of 10,000) of the trials return a power below 12.19. Thus, this 99th percentile level is plotted as the horizontal black line on Figure 2b. The position of the vertical dot-dashed blue line relative to the red cumulative distribution curve in Figure 2d shows that the highest power measured from the *real* data is far above what would typically be expected to emerge from analysis of any random distribution of photons.

3.4. Applying Rayleigh Testing and Monte Carlo Simulation to Heritage Data Sets

Following the exposition of our method to search for quasi-periodic signals in jovian X-ray data, we now wish to apply this technique to the full catalogue of pre-Juno era Chandra data (see Figure 1 and Table 1). The results of our timing analysis of all Chandra observations between 1999 and 2015 are summarized in Figure 3. The top panel of this figure shows the total number of photons recorded by the Chandra HRC detector during the various observations (ObsID numbers at the bottom of the plot). There is significant variability in these photon numbers, and at least some of that is due to the fact that observations last from 18 to 72 ks. The second panel represents an effort to normalize these photon counts, by defining the length of the *hot spot visibility window* as per the method outlined in section 2 above, counting the photons that arrived

Table 2
Table of Heritage Data Sets for Which We Conducted Timing Analysis

Telescope-Instrument-Region	Start date (year-month-day hr:min:s)	Dur. of full obs.	Obs ID	Total counts	Sig. percentile	Sig. *p* value	Best period (min)
Chandra-HRC-I North-All	2000-12-18 09:53:23	36 ks (600 min)	1862	664	75.2	0.2477	12.1
Chandra-HRC-I North-HS	2000-12-18 09:53:23	350 min HS window	1862	521	62.2	0.3784	2.1
Chandra-HRC-I North-HS	**2000-12-18 09:53:23**	**Spatial selection: 5° radius circle center on lat 65° lon 170°**	**1862**	**113**	**99.5**	**0.0052**	**45.96**
Chandra-HRC-I South-All	2000-12-18 09:53:23	36 ks (600 min)	1862	163	77.6	0.2238	3.8
Chandra-ACIS-S North-All	2003-02-24 15:36:22	30 ks (500 min)	3726	229	42.8	0.5721	20.7
Chandra-ACIS-S South-All	2003-02-24 15:36:22	30 ks (500 min)	3726	130	93.5	0.065	2.92
Chandra-HRC-I North-All	2003-02-25 00:21:20	72 ks (1,200 min)	2519	790	92.4	0.0763	12.6
Chandra-HRC-I North-HS1	**2003-02-25 00:21:20**	**300 min HS window**	**2519**	**303**	**99.94**	**0.0006**	**33.1**
Chandra-HRC-I North-HS2	2003-02-25 00:21:20	465 min HS window	2519	401	91.2	0.0885	12.7
Chandra-HRC-I South-All	2003-02-25 00:21:20	72 ks (1,200 min)	2519	669	60.0	0.3998	36.2
Chandra-HRC-I South-HS1	2003-02-25 00:21:20	300 min HS window	2519	229	16.2	0.8379	3.4
Chandra-HRC-I South-HS2	2003-02-25 00:21:20	420 min HS window	2519	335	71.1	0.2888	27.4
Chandra-ACIS-S North-All	2003-02-25 20:16:52	41 ks (683 min)	4418	289	33.4	0.6659	32.7
Chandra-ACIS-S North-HS	2003-02-25 20:16:52	350 min HS window	4418	228	96.1	0.0392	21.9
Chandra-ACIS-S South-All	2003-02-25 20:16:52	41 ks (683 min)	4418	188	88.7	0.1135	2.2
Chandra-ACIS-S North-All	2007-02-08 08:29:44	18 ks (300 min)	7405	148	95.8	0.0417	6.3
Chandra-ACIS-S South-All	2007-02-08 08:29:44	18 ks (300 min)	7405	32	87.1	0.1288	10.1
Chandra-ACIS-S North-All	2007-02-10 19:53:21	18 ks (300 min)	8216	170	30.2	0.6980	2.5
Chandra-ACIS-S South-All	2007-02-10 19:53:21	18 ks (300 min)	8216	57	53.5	0.4647	2.4
Chandra-ACIS-S North-All	2007-02-24 21:23:16	18 ks (300 min)	8217	219	87.2	0.1285	4.8
Chandra-ACIS-S South-All	2007-02-24 21:23:16	18 ks (300 min)	8217	37	80.4	0.1959	2.2
Chandra-ACIS-S North-All	2007-03-08 21:02:26	18 ks (300 min)	8218	248	26.3	0.366	5.8
Chandra-ACIS-S South-All	2007-03-08 21:02:26	18 ks (300 min)	8218	27	n/s		
Chandra-ACIS-S North-All	2007-03-03 07:41:28	18 ks (300 min)	8219	46	25.8	0.7418	96.8
Chandra-ACIS-S South-All	2007-03-03 07:41:28	18 ks (300 min)	8219	88	79.0	0.2103	3.2
Chandra-ACIS-S North-All	2007-03-07 14:17:52	18 ks (300 min)	8220	80	88.3	0.1174	3.1
Chandra-ACIS-S South-All	2007-03-07 14:17:52	18 ks (300 min)	8220	41	87.3	0.1274	4.8
Chandra-ACIS-S North-All	**2011-10-02 21:54:26**	**40 ks (667 min)**	**12315**	**548**	**99.33**	**0.0067**	**23.5**

Table 2 *(continued)*

Telescope-Instrument-Region	Start date (year-month-day hr:min:s)	Dur. of full obs.	Obs ID	Total counts	Sig. percentile	Sig. *p* value	Best period (min)
Chandra-ACIS-S North-HS	2011-10-02 21:54:26	350 min HS window	12315	394	97.44	0.0256	26.3
Chandra-ACIS-S South-All	2011-10-02 21:54:26	40 ks (667 min)	12315	201	86.2	0.1382	38.0
Chandra-ACIS-S North-All	2011-10-04 14:33:08	40 ks (667 min)	12316	352	61.8	0.3821	6.2
Chandra-ACIS-S North-HS	2011-10-04 14:33:08	350 min HS window	12316	234	50.9	0.4911	2.6
Chandra-ACIS-S South-All	2011-10-04 14:33:08	40 ks (667 min)	12316	168	41.5	0.5894	2.4
Chandra-HRC-I North-All	**2014-04-08 08:18:10**	**40 ks (667 min)**	**15671**	**653**	**99.6**	**0.0037**	**12.4**
Chandra-HRC-I North-HS	2014-04-08 08:18:10	350 min HS window	15671	489	94.0	0.0599	22.4
Chandra-HRC-I South-All	**2014-04-08 08:18:10**	**40 ks (667 min)**	**15671**	**190**	**99.99**	**0.0001**	**34.9 (Secondary broad peaks ~14 and ~41 min)**
Chandra-HRC-I South-HS	**2014-04-08 08:18:10**	**270 min HS window**	**15671**	**141**	**99.99**	**0.0001**	**14.1 (Secondary broad peaks ~35 and ~41 min)**
Chandra-HRC-I North-All	2014-04-10 01:09:23	40 ks (667 min)	16299	587	94.9	0.0509	2.9
Chandra-HRC-I North-HS	2014-04-10 01:09:23	347 min HS window	16299	516	76.4	0.2362	12.4
Chandra-HRC-I South-All	2014-04-10 01:09:23	40 ks (667 min)	16299	128	8.3	0.917	18.4
Chandra-HRC-I North-All	2014-04-12 22:09:30	40 ks (667 min)	15672	529	98.0	0.0196	8.0
Chandra-HRC-I North-HS	**2014-04-12 22:09:30**	**350 min HS window**	**15672**	**400**	**99.35**	**0.0065**	**8.0**
Chandra-HRC-I South-All	2014-04-12 22:09:30	40 ks (667 min)	15672	175	98.3	0.0174	24.0
Chandra-HRC-I South-HS	2014-04-12 22:09:30	240 min HS window	15672	108	96.5	0.0355	6.6
Chandra-HRC-I North-All	2014-04-15 20:43:04	40 ks (667 min)	15669	481	64.0	0.3596	2.9
Chandra-HRC-I North-HS	2014-04-15 20:43:04	350 min HS window	15669	392	56.7	0.4327	9.8
Chandra-HRC-I South-All	2014-04-15 20:43:04	40 ks (667 min)	15669	172	23.6	0.7644	14.96
Chandra-HRC-I North-All	2014-04-17 12:19:31	40 ks (667 min)	16300	339	38.0	0.6204	28.5
Chandra-HRC-I North-HS	2014-04-17 12:19:31	362 min HS window	16300	267	50.1	0.4994	28.2
Chandra-HRC-I South-All	2014-04-17 12:19:31	40 ks (667 min)	16300	139	65.0	0.3498	2.2
Chandra-HRC-I North-All	2014-04-20 02:19:30	40 ks (667 min)	15670	179	39.8	0.6017	9.2
Chandra-HRC-I South-All	2014-04-20 02:19:30	40 ks (667 min)	15670	141	63.0	0.3703	14.7

Note. Observations with quasi-periods above the 99.0% significance threshold (*p* value 0.01 or lower) are shown in bold red text. List of Chandra observations of Jupiter's X-rays from 1999 to 2015 (all pre-Juno era). Column 1 gives the observation instrument and then region (North or South, and *All* or *HS*—hotspot). The following columns give the observation start date, the duration of the entire observation in kilosecond or minutes, the Chandra ObsID, and the total counts recorded during that interval. We note that the hot spot intervals are of shorter duration than the All North or South intervals, and thus, where appropriate, we quote the number of 60-s bins included in the hot spot visibility region. The final columns give the outputs of Rayleigh analysis for the top peak, listing the (i) significance from the Monte Carlo simulation as a percentile, (ii) significance as a *p* value, (ii) best quasi-period associated with the highest power peak. HRC = High-Resolution Camera; ACIS = Advanced CCD Imaging Spectrometer.

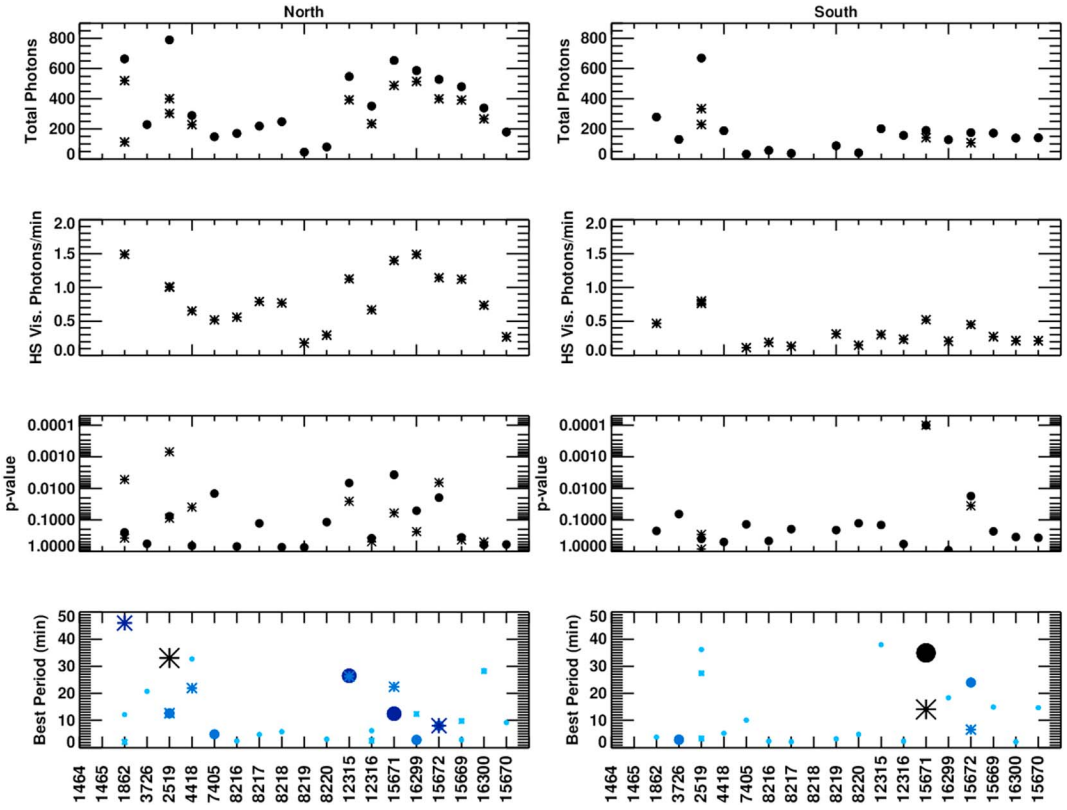

Figure 3. Figure summarizing the results of Rayleigh and Monte Carlo analysis of all Chandra observations listed in Table 1 (with more detailed results listed in Table 2), with ObsIDs listed on the *x* axis of the bottom panels. The left-hand column shows results for the north, while the right-hand column shows results for the south. The top panels show the total photon counts, while the second row shows the number of photons normalized to hot spot visibility intervals. Filled circles denote results for the entire observation interval, while the asterisks denote the results for the hot spot visibility region only (hence, always lower counts for these examples). The third row shows the *p* values associated with each observation (smallest, most significant *p* values at the top), while the associated quasi-periods are then plotted in the bottom panel. Symbol size and darkness is inversely proportional to the *p* value, such that more significant (smaller *p* value) periods are shown as larger, darker symbols, with colors from black through to light blue with decreasing significance.

during this window, and dividing one number by the other to get a rate of photons per minute during the hot spot visibility window (the most active interval during any observation). One long observation (2519) has two hot spot visibility windows. It should be noted that for some observations (e.g., ObsIDs 7405, and 8216–8220) where the total observation duration is 18 ks, no down-select of hot spot window has been conducted: counts were low across these intervals, and several of the observations were planned and optimized to cover only the fractions of Jupiter rotations when either the northern or southern hot spot was visible. These top two panels show considerable variability in X-ray photon rates. The down-selection of hot spot visibility windows illustrates that both northern and southern hot spot regions are strong, relatively concentrated sources of X-ray photons, with northern emission rates on average higher than the south.

Timing analysis was conducted on all observation intervals, with results summarized in Table 2. For each observation the corresponding Rayleigh test returned a peak power, with associated best period. The significances of these periods were then calculated from the Monte Carlo analysis as outlined in section 3.2 above. The third panel of Figure 3 shows the range of *p* values associated with these maximum powers from Rayleigh analysis. It is clear that there are a very small number of examples with *p* values of 0.01 or smaller, with the majority of events clustered with *p* values of between 0.01 and 1. The bottom panel shows the *best* periods associated with the peak power from the Rayleigh test for each observation. Larger, bolder symbols denote lower *p* values, with the intention to draw the eye to these most significant cases.

The five most significant quasi-periods for the north (based on their corresponding *p* value) are ~45.96 (ObsID 1862, strict spatially selected hot spot), ~33.1 (ObsID 2519, hot spot visibility window), ~23.5 (ObsID 12315, for

all northern auroral photons), ~12.4 (ObsID 15671, all northern auroral photons), and ~8.0 min (ObsID 15672, for the hot spot visibility window). The two most significant quasi-periods for the south are from the same observation: ~34.9 and 14.1 min (ObsID 15671, all southern auroral photons and hot spot visibility window, respectively. There are secondary significant peaks in the periodogram for the full southern auroral region at ~14 and ~41 min and for the southern hot spot at ~35 and ~41 min indicating that these three quasi-periods could be important for this observation). All of the above are significant at or above the 99th percentile (p values of 0.01 or lower). If we lower this significance threshold to include other candidate observations with significances above the 90th percentile (p value <0.1), we find eight further examples for the north, and three further examples for the south. This may be instructive, particularly if we find additional occurrence of the same or very similar periods: for the north this expanded candidate catalogue of 13 observations (with $p < 0.1$) contains three instances of an ~12- to13-min period, two instances of an 8-min period, and three instances of an ~22- to 23-min period. Most of these duplicate periods represent intervals where one observation covers the entire northern auroral region and the other covers the hot spot visibility region: this repetition of periods for given observation intervals is most likely to equate to the hot spot dominating rather than to the conclusion that there is any particular period which is common across multiple distinct observations. However, we must exercise caution in considering events which would not meet any typical standards of statistical significance: for N tests, we expect of order $N*p$ false positives when adopting a critical value of p. For example, a set of 50 tests would give 5 false positives for a p value threshold of 0.1. Thus, we believe that for the set of heritage Chandra observations presented in this work and illustrated in Figure 3, p values of 0.01 give at best marginal detections, and p values of 0.1 or greater are unlikely to be statistically significant. The third row of Figure 3 clearly shows a large separation between the most significant periods ($p < 0.01$) and the rest of the catalogue.

There are several features from Figure 3 which are worth highlighting. First, we note that quasi-periodicity can be drawn out by making a strict selection on hot spot visibility, either through the method outlined in section 2 above, or through selecting a smaller region in latitude-longitude from a polar projection (as done by G02 in their discovery of the northern hot spot with ObsID #1862). It is important to note that when quasi-periodicity analysis was carried out on the entire interval for ObsID #1862, from 18 December 2000, no significant peak was found. It was only when the strict down-select of hot spot photons was performed that a statistically significant (p value < 0.01) quasi-period emerged from the analysis. This could maybe suggest that there was a particularly high quantity of scattered solar photons increasing the noise of the data or that there are multiple X-ray sources in the Northern aurora and only one of these is associated with periodic behavior (as suggested in D17).

The second interesting feature from Figure 3 is that there can be significant rotation-to-rotation variability in the Jovian X-ray emission. A long (72 ks) observation was performed on 25 February 2002 (ObsID 2519), spanning two rotations of the planet Jupiter. Analysis of the entire northern auroral zone photons returned a quasi-period of ~12.6 min with a significance of 92.4% (p value 0.0763). When the two rotations were split and the hot spot visibility regions from orbits 1 and 2 were analyzed separately, the behavior from one rotation to another was found to be rather different. As shown in Figure 1, the hot spot visibility window from the first orbit displayed an ~33.1-min quasi-period with a statistical significance from Monte Carlo modeling of 99.94% (p value of 0.0006). Analysis of the auroral X-ray photons from the next rotation returned a best quasi-period of ~12.7 min (almost exactly matching the quasi-period for the entire region), but with a lower significance of 91.2% (p value of 0.0885). The observation which precedes this interval (ObsID 3726) does not return anything close to a statistically significant period from the north, while the observation following the ObsID 2519 interval (ObsID 4418) returns a quasi-period from the northern hot spot of ~21.9 min with significance of 96.1% (p value 0.0392). Our overall impression of these three observations (3726, 2519, 4418) is that the northern hot spot quasi-period of ~33.1 min highlighted in Figure 2 (from first part of ObsID 2519) was significant beyond doubt, while the variable and more marginal detections of quasi-periods in the surrounding time intervals may hint at a sporadic pulsing process. In total, these three observations span 143 ks, and we refer the reader to Elsner et al. (2005) for a detailed analysis of how these observations compare to simultaneous UV observations of Jupiter.

The third feature to note from Figure 3 is that the counts from the south are consistently lower than from the north, primarily due to viewing constraints during many of the observations. For the south, the visibility mostly covers the region which has been termed from UV observations the *noon active region*, whereas

the observations of the north typically cover this as well as the dusk active region and the swirl region. The hot spot intervals for both north and south were extracted as per the method outlined in section 2, but there were several observations (particularly during observation campaigns in 2007) where the counts were too low to down-select any further as timing analysis on such sparse counts would not give any meaningful results (particularly true for southern observations). Qualitatively speaking, the northern hot spot region is much easier to select than any similar feature in the south, as the northern hot spot dominates the photon count. Thus, there are far fewer southern hot spot selections (shown by asterisks) in the top right-hand panel of Figure 3 than there are northern hot spot selections on the left. Nonetheless, the south can, at times, be very active: in the work published by D17 from an observation campaign in 2016 (outside of the range of this work), the southern hot spot was clear and the pulsation was statistically significant. Future work should focus on statistical examination of the spatial spread of X-ray photons across the northern and southern auroral regions, and exploration of the conditions under which the emission is concentrated into clear hot spots, plus the varying location and extent of these regions.

Finally, intervals where there was good viewing of both north and south during the same planetary rotation should be analyzed in more detail. Take for example ObsID 15671 (8 April 2014), where our analysis returns statistically significant periods from both the north and south. The quasi-periods differ between hemispheres: the northern auroral region and northern hot spot region return quasi-periods of ~12.4 and 22.4 min, while in the south the broad southern emission exhibits a quasi-period of ~34.9 min (with broader significant peaks at ~14 and ~41 min), compared to its more concentrated hot spot which shows a sharp peak at a period of ~14.1 min (with broader significant peaks at ~35 and ~41 min). Examining hemispheric differences in detail could help to shed light on the as yet unknown drivers of the X-ray emission.

Detailed numbers to accompany this analysis are given in Table 2, which quotes counts, significances, and best quasi-periods. The supporting information also includes a figure for each of the observations with north, south, and hot spot selections shown separately.

3.5. Impact of Smoothing on the Validity of Statistical Tests

The summary Table 2 and Figure 3 above illustrate that statistically significant quasi-periods in jovian X-ray emissions are relatively rare. One of the most commonly cited (and searched-for) quasi-periods is the ~45-min period reported in G02 for the Chandra data set obtained on 18 December 2000 (ObsId 1862). Our Rayleigh analysis recovers this signal, but at a far lower statistical significance ($p = 0.0052$) than suggested in G02 ($p = 4 \times 10^{-6}$). It is instructive to explore the reason for this dramatic difference in the confidence we assign to this signal. In Figure 4 we examine the interval of data that yielded this result, and show that the way the input light curve data are treated can have a large impact on the emerging statistical significances. Specifically we focus on (i) how smoothing the input light curve before timing analysis can result in artificially inflated statistical significances being inferred (unless the smoothing is carefully accounted for in the statistical testing procedure) and (ii) how small differences in hot spot selection can alter the resulting quasi-periodicities markedly. In order to allow a direct comparison with the analysis carried out in G02, we take as our starting point the light curve binned into 60-s time bins. Because of the nature of these input data sets, we cannot run Rayleigh testing (which demands unbinned, individually tagged photon arrival times as input), and thus we instead use Lomb-Scargle analysis for this section, but still extracting significances from Monte Carlo simulation. The Lomb Scargle analysis searched 150 equally logarithmically spaced steps between periods of 2 and 200 min.

The data from this observation were taken by the Chandra HRC-I instrument on 18 December 2000 from 09:53. The observation took place over 36 ks, and here we focus on the data from the north polar hot spot region. For this section, instead of taking a hot spot visibility window as per the analysis in the rest of this paper, we applied the same strict spatial restriction as in G02 to select the hot spot: a 5° radius circle centered on a longitude of 170° and latitude of 65°. This spatial restriction returned a total of 113 X-ray photons, as in the original Gladstone work. Figure 4a shows the original light curve, with X-ray photons from the northern hot spot region (113 photons) binned into 60-s bins (time 0 is the time at which the first hot spot photon was registered, and such photons appeared over a window ~263 min long). The quantized nature of the emission is evident (and emphasized by the plotting style of asterisks for photon counts joined by solid lines), with many times where no photons were observed at all.

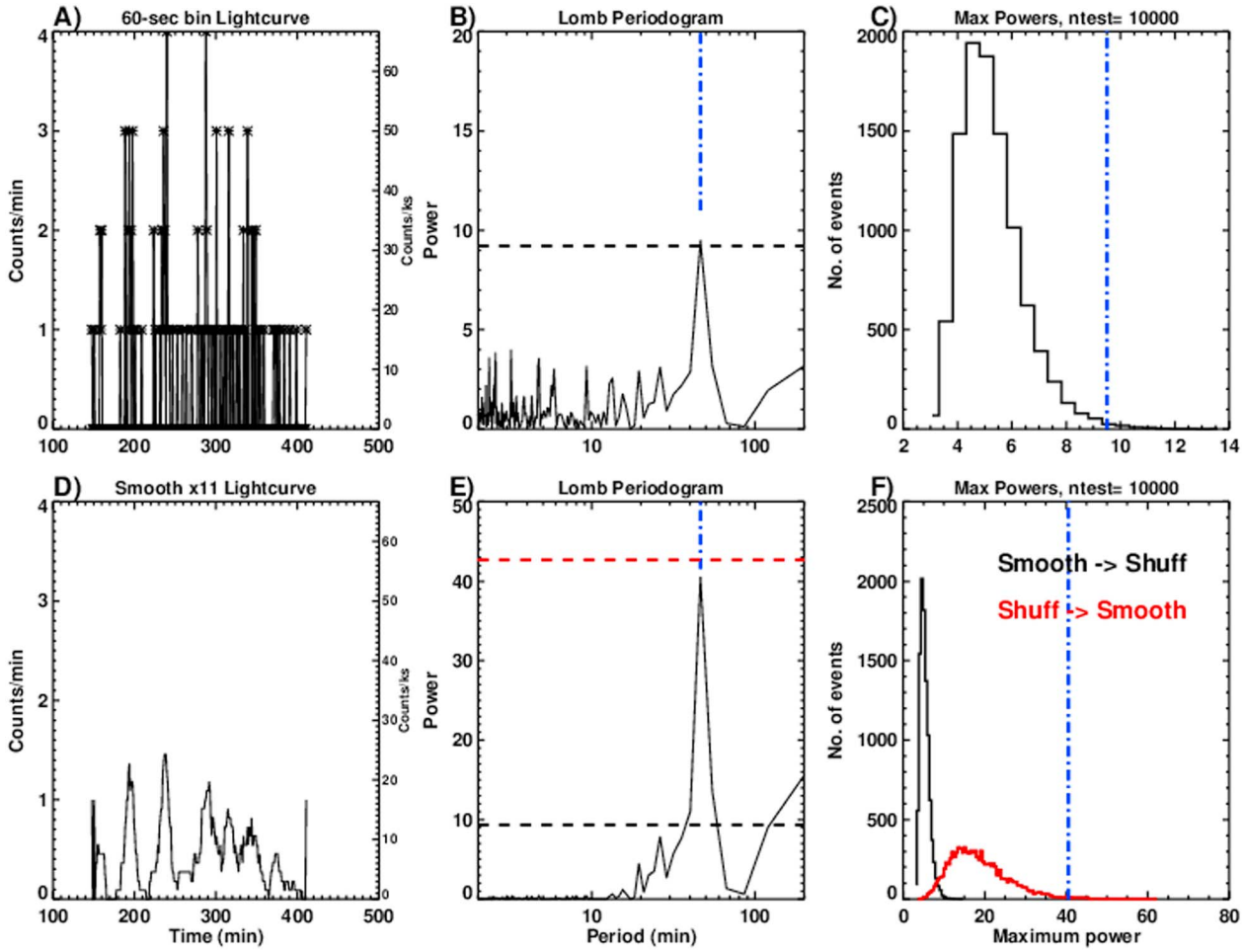

Figure 4. Light curves and timing analysis of X-ray photons from Jupiter's northern auroral hot spot measured by Chandra during 18 December 2000 from 09:53. (a) Light curve of 60-s binned data, with time of the first recorded hot spot photon set to 0 min (b) Lomb-Scargle Periodogram of light curve in panel (a). Peak power (associated with *best* quasi-period) marked by vertical dot-dashed blue line. Power associated with 99th percentile of 10,000 Monte Carlo simulations marked by horizontal black dashed line. (c) Histogram of maximum powers from Lomb-Scargle analysis of 10,000 randomly shuffled light curves based on original data. Peak power (associated with best quasi-period of original 60-s binned data) marked by vertical dot-dashed blue line. (d)–(f) Same format as (a)–(c) but now for a smoothed version of the 60-s binned light curve. Smoothing was carried out via an 11-point (660-s) boxcar filter. The black and red histograms in panel (f) correspond to the maximum peak powers obtained from mock data sets constructed in two different ways. For the black histogram, the binned and smoothed real data was only randomly shuffled before calculating the Lomb-Scargle power spectrum. For the red histogram, the binned and smoothed real data were first randomly shuffled and then smoothed (again using an 11-point boxcar filter) before calculating the Lomb-Scargle power spectrum. Smoothing induces correlations in the real data that must be taken into account in constructing valid mock data. These correlations are missing from the mock data associated with the black histogram, but are present in the mock data associated with the red histogram. As a result, estimating *p* values from the black histogram would suggest far too high a statistical significance for any putative period signal. The red horizontal line in panel (e) corresponds to the power associated with the 99th percentile of 10,000 shuffled then smoothed light curves.

Computing the Lomb-Scargle power spectrum directly from the 60-s binned data set produces a peak power of 9.5 at a quasi-period of ~46.3 min (Figure 4b). The black horizontal dashed line shows the 99% confidence ($p = 0.01$) level obtained from Monte Carlo simulations. This corresponds to a power of 9.2, so both this Lomb-Scargle analysis and the Rayleigh analysis (Table 2) suggest a statistical significance of $p = 0.01$ for this signal. Figure 4c shows the results of the Monte Carlo analysis in a similar format to Figure 2, whereby we used a random number generator to shuffle the binned photons around in time, thus destroying any inherent quasi-periodicities, and then ran the Lomb-Scargle analysis on the shuffled fake data. This randomization (shuffling) test has the advantage of being distribution-free. An alternative method would be to randomly redistribute the counts in time, for example, assuming a uniform distribution. For our example, both methods provide almost identical results. After 10,000 runs we stored the maximum power associated with the best quasi-period in each case and the histogram of these maximum powers is shown in Figure 4c. As in

Figure 4b, the vertical dot-dashed blue line shows the power of the highest peak from the analysis of the original 60-s binned data. Thus, our Lomb-Scargle and Monte Carlo timing analysis of 113 photons from a strict spatial selection of Jupiter's northern hot spot region during this observation has yielded a best quasi-period of ~46.3 min with a significance of 99.28% (peak in Figure 4b above the 99th percentile horizontal black line, p value = 0.0072).

When similar analysis is conducted on a smoothed input data set, problems and inaccuracies with the time series analysis emerge. Smoothing equates to information loss, and the aim of our analysis in Figures 4d–4f is to explore the results we would get if our starting point was smoothed data. By comparing and contrasting these against Figures 4a–4c (on original binned data, where we have more complete information and no inappropriate long-range correlations), we can more easily see how smoothing can lead us to incorrect conclusions and inflated significances. It is common practice to smooth data for the presentation of light curves, and here we have used the IDL smooth function, which takes a boxcar average, in this case over a time step window of 11 min. The resulting smoothed light curve in Figure 4d is much more suggestive of a quasi-periodicity than the unsmoothed one, and the associated Lomb-Scargle power spectrum (Figure 4e) also looks impressively clean, with a maximum peak power of over 40 at the period of ~46.3 min. The horizontal black line in Figure 4e is the same as that in Figure 4b, and denotes the 99% confidence level from the Monte Carlo simulations, corresponding to a power of 9.2.

The significance inferred from Figure 4e is not correct: it is based on an inappropriate (smoothed) input data set which violates the fundamental tenets of the time series analysis. The difference that the smoothing has made is to (i) trick the eye into seeing clusters of count peaks which were not evident from the unsmoothed, highly quantized input data, (ii) artificially amplify a moderately significant signal to make it appear more significant. Smoothing results in irreversible information loss and should only be conducted for illustrative purposes: periodicity analysis should always be conducted on raw input data. Perhaps the most dangerous (from a statistical perspective) aspect of the smoothing is that, by definition, it introduces correlations between adjacent points, calling into question the results of analyses such as Lomb-Scargle which are designed to be carried out on completely independent data points. Unless great care is taken, these correlations can wreak havoc on Monte Carlo significance tests, since these are usually designed to work on uncorrelated input data.

The true impact of the smoothing is made most clear in Figure 4f which is in a similar format to Figure 4c and shows the results of Monte Carlo testing. In this case the smoothed northern hot spot data set has been treated in two distinct ways. First, the smoothed input data have been shuffled and these mock data sets run through the Lomb-Scargle analysis 10,000 times. The distribution of maximum powers (associated with best quasi-periods) is shown by the black curve in Figure 4f which is very similar to the black curve in Figure 4c (both representing 10,000 runs on shuffled data). The main difference emerges when the 99th percentile levels from these black curves are compared to the periodograms in Figures 4b and 4e: the periodogram of the unsmoothed data in Figure 4b yields a highest peak just above the 99th percentile significance cutoff, whereas the periodogram of the smoothed data in Figure 4e yields a highest peak far above the 99th percentile significance cutoff. This later significance level is artificially inflated for the reasons outlined above and should not be used.

We can go one step further to illustrate the impact of smoothing: in Figure 4f the red curve shows the distribution of 10,000 runs where the smoothed light curve from Figure 4d has been shuffled and then smoothed, with Lomb Scargle analysis conducted on the smoothed data. This ensures that smoothing-induced correlations are present in both the real and the mock data. It is immediately clear from the red histogram that the maximum peak powers found in the Lomb-Scargle power spectra of these mock data sets are much higher than those obtained from the unsmoothed mock data sets. As a result, the (correct) statistical significance is much lower (99th percentile curve associated with red histogram is shown as a red horizontal dashed line in Figure 4e), and once again in line with our Rayleigh analysis (Table 2) and the Lomb-Scargle analysis in Figures 4a–4c.

In summary, input data should not be smoothed before conducting periodicity analysis. However, for illustration, this second method of data treatment (smoothing the shuffled data) shows how Monte Carlo testing could proceed if the input data were smoothed for any reason. The key here is that the mock data sets upon which the Monte Carlo analysis is conducted should resemble the real data as closely as possible. Thus, if the

periodogram (as in Figure 4e) operates on smoothed data, then the simulations should also operate on smoothed data, to infer significances appropriately. In this case (red curve in Figure 4f), the smoothing of the shuffled data introduces the long-range correlations which were introduced by the smoothing of the real data in light curve in Figure 4d and the associated Lomb Periodogram in Figure 4e. The red curve thus shows the formally correct way to estimate significance from smoothed data. The red horizontal line in Figure 4e represents the 99th percentile significance threshold for the smoothed simulation runs, and thus the relevant threshold against which to compare the peak power from the Lomb-Scargle analysis of the smoothed data. The peak power from the Lomb analysis of the smoothed light curve lies below this red line, indicating that the effect of the smoothing is, in effect, to reduce the power of the test.

Overall, our results from Figure 4 show that it is inappropriate to smooth a data set before conducting Lomb-Scargle analysis because it introduces long-range correlations which can of themselves invalidate the periodicity tests, but also because smoothing artificially enhances moderately significant signals and yields peak powers post-Lomb-Scargle-analysis that appear to be more strongly significant than they truly are.

4. Discussion

The results of our exploration of heritage Chandra Jupiter observations reveal several important features in the X-ray emission which must be accounted for when conducting timing analysis.

First, it is critical to note that the results of timing analysis are highly sensitive to the selection of the region for analysis. The auroral photons are much more concentrated than those from the disk, and thus we have employed a manual region selection method to extract the northern and southern auroral regions. We have then used the NASA JPL HORIZONS program to select viewing windows during which the auroral hot spots are expected to be visible (longitudes of 155–190° for the north and 0–75° for the south). There is an alternative method to select the northern (or southern) hot spot regions: the raw data are transformed into a frame which accounts for Jupiter's motion across the sky; these photons are in turn distributed over the sky using a 2-D Gaussian for the point spread function; A criterion is set for this point spread function ($>$0.3) in order for photons which may appear near the limb to be tagged as from Jupiter; these time-tagged photons are mapped into jovian latitude and system III longitude coordinates, and a spatial selection in latitude and longitude is conducted. This method was used for the data displayed in Figure 4. A detailed comparison of the various region selection and mapping techniques is beyond the scope of our current focus (and may be the subject of a future study), but throughout our work it became very evident that the results of timing analysis are highly sensitive to the selection of the hot spot region. Definitions have been put forward (e.g., originally by G02 for the north, and D17 for the south) which describe the hot spot location for individual observations. For this work we have chosen to adopt the NASA JPL HORIZONS visibility window selection method, noting the caveat that these observation windows should be dominated by hot spot emission but may also contain a small fraction of non-hot spot auroral photons. Future work on a case-by-case basis should perhaps quantitatively explore the density of points as distributed across the northern and southern polar regions and place a numerical criterion on the clustering of photons to define a bespoke hot spot for each observation and explore variability therein. This will complement and extend the work of Kimura et al. (2016) who defined a *core* and *halo* region for the northern hot spot. Mapping the hot spot region out to the magnetosphere with magnetic field models (e.g., Vogt et al., 2015) should help to shed more light on the physical driver by pinning down the location of the X-ray source (including careful consideration of the limitations of mapping near the outer magnetosphere and boundary with open field line regions). Various driver scenarios such as the Kelvin-Helmholtz instability and pulsed dayside reconnection have specific location constraints in terms of the source of initial particle acceleration, and mapping, combined with in situ spacecraft data will allow significant progress in probing the question of X-ray driver.

The relatively rare detection of significant quasi-periodicity over all observations may also provide some clues as to the nature of the X-ray emission driver. Where single-trial statistically significant quasi-periodicity is present in the north it is often concentrated into the hot spot visibility region as opposed to the broader auroral zone. This suggests that whatever physical mechanism is responsible for driving quasi-periodic X-ray emission must itself be restricted to act only along the precipitating flows of charged particles responsible for the hot spot (rather than more broadly across the entire auroral region). The relationship between the southern hot spot as compared to the broader southern auroral region is less clear, in part due to poorer viewing of

the south and the resultant small number statistics on significant quasi-periods. The contours of the magnetic field at Jupiter (e.g., Vogt et al., 2015) may make it easy to understand how X-ray photons are concentrated into a hot spot in the north, while Elsner et al. (2005) and Branduardi-Raymont et al. (2007) both noted that the southern X-ray aurora is more diffuse than its northern counterpart. A larger hot spot area in the south (e.g., D17) relative to the north may cause any inherent periodicity in the south to smear out and thus be more difficult to detect with high degrees of significance. Moreover, viewing orientation is critical, and robust examinations of north/south conjugacy must take place under similar observation conditions for north and south. Hemispheric differences emerge from our statistical analysis: In the example of ObsID 15671 (8 April 2014), conjugate observations of the north and south yield statistically significant quasi-periods from both regions (~12.4 and ~22.4 min at 99.6% and 94.0% significance from the northern auroral region and hot spot, respectively, and sharp peaks at ~34.9 and ~14.1 min at 99.99% significance for each from the southern auroral region and southern hot spot, with broader significant peaks centered around ~14, ~35, and ~41 min). Future work should focus on case studies such as this where the north and south appear to pulse independently (and instances of multiple candidate quasi-periods): we need to understand the asymmetric and variable nature of X-ray driving at Jupiter. Nonconjugacy of emission (also reported in D17) may point more toward physical processes which take place on open field lines, or may simply come about due to asymmetries in ionospheric conductivities or magnetic field strengths. In situ Juno data to accompany X-ray campaigns may help to discriminate between different scenarios.

A further caveat related to hot spot selection is that for any given hot spot visibility window, the hot spot area changes as it moves across the disk. This was noted by G02 who plotted a projected area of the hot spot (as a percentage of the projected area of Jupiter) on their light curve. This hot spot motion means that the probability of detecting a photon is not the same in every time bin. We have not accounted for this in our quantitative timing analysis, but it is likely to have an impact on the significance of the quasi-periods. Furthermore, it is also possible that the physical shape of the hot spot changes as the planet rotates, depending on changes in the magnetosphere which map to this auroral region.

This work focuses on data from Chandra only, but there are several cases where there are contemporaneous XMM data. D17 published work to unveil a statistically significant quasi-period from the southern hot spot of ~11 min, which was confirmed by both Chandra and XMM observing at the same time. Such cases of repeated (multitrial) detections add to the confidence in these statistically significant quasi-periods.

Many of the intervals that we have examined display relatively low count rates, and highly quantized light curves, with many intervals of zero detection followed by sporadic X-ray emission. Some traditional timing analysis methods have limitations when dealing with such a sparse count regime. Furthermore, binning sparse data into long time bins before conducting analysis (such as Lomb-Scargle) means that shorter periods are less likely to emerge from the analysis. Smoothing the input data before timing analysis invalidates the results as it violates the assumption that points are independent, and yields artificially inflated statistical significances. We suggest that the optimum method for timing analysis of such data is to apply Rayleigh testing of the time-tagged photons and Monte Carlo simulation to extract significances. We have provided code in both Python and IDL as supporting information to accompany this paper so that others can explore the power of this test. We feel it may have particular potential for comparing X-ray data with UV emissions, which at Jupiter have been reported to have periods ranging from ~10 min (Nichols et al., 2017) down to ~2–3 min (Bonfond et al., 2011).

Comparison with the UV data in particular has enormous potential to unveil new information about the dynamics of Jupiter's auroral zone. It is important to note some key features of the observed quasi-periodic flaring from the UV; namely, that quasi-periodic flaring has been observed in only approximately half of observations, and, when found, the flares may often pulse for only approximately half of a given 45-min Hubble observation window (Bonfond et al., 2016). The observation windows that we are considering for the X-rays here are on the order of ~5–20 hr, during which the Chandra detector typically receives on order a few hundred photons at most. With future contemporaneous X-ray and UV observations we may consider whether the sporadic UV flaring behavior could go some way to explaining why so few (relatively long) X-ray sequences display strongly statistically significant quasi-periods. The Rayleigh test is our best chance (given no requirement for binning, and thus no information loss) at exploring shorter observation windows in the X-rays and being in a position to more directly compare the X-ray and UV wavelengths.

Where statistically significant quasi-periods are detected, they are quite variable, and can even show rotation-to-rotation variability. For example, during ObsID 2519 (25 February 2003) which lasted 72 ks (~2 Jupiter rotations), the northern hot spot was visible on both rotations. During the first visibility window the analysis yielded an ~33.1 min quasi-period with statistical significance of 99.94% (p value 0.0006), whereas on the second viewing several hours later the highest peak period was ~12.7 min, but with a statistical significance of only 91.2% (p value 0.0885). As such, it appears that, where present, quasi-periodic signals may not remain coherent over intervals of longer than 5 hr. However, this is just one example of a long duration observation which enabled us to search for rotation-to-rotation variability and coherence of signal. Most of the other observations cover just a single planetary rotation, with timescales of days to years between adjacent observations. This provides motivation for the proposal (and execution) of further campaigns which cover multiple consecutive planetary rotations, to understand how conditions can change over timescales of hours.

Finally, while we have focused on the lowest p values to determine the most statistically significant quasi-periods, in section 3.4 above we have briefly considered whether particular quasi-periods (perhaps with lower significances) emerge multiple times from separate observations. With the catalogue currently available to us, we do not see a particular candidate quasi-period (for either north or south) that is striking in terms of common occurrence. Neither do we see obvious quasi-periods which are harmonics of each other. Future searches, in parallel with development of theoretical frameworks to test X-ray generation mechanisms should help us to focus on particular quasi-periods which tie well with the timescales of possible drivers. It may be the case that future analysis of X-ray data in concert with other contemporaneous data sets (such as time-tagged UV photons) may shed light on the reasons for such low significances for many of the X-ray observations. These may include drifting frequencies, signals which are only regular for short intervals, secondary phenomena which may interfere with the main driver of pulsing (leading to missing or additional beats), or a signal which is composed of short bursts rather than a smooth curve. These nonperiodic but nonrandom features may still pose interesting questions for jovian physics.

5. Summary

The large catalogue of observations of Jupiter's X-rays includes long observations (multiple planetary rotations) and successive observations relatively closely spaced in time. These features combine to allow us to pursue advanced methods for examining temporal patterns in the X-ray emission and particularly allow us to search for quasi-periodic phenomena. Previous works have reported individual observations of significant quasi-periodic emissions emerging from the jovian system in X-ray, UV, and radio wavelengths.

In this paper we have explored Chandra observations of Jupiter's X-ray emissions from 1999 to 2015, with a focus on the search for statistically significant quasi-periods. Overall, we find that statistically significant quasi-periodicities in jovian auroral X-ray emissions are relatively rare. The treatment of the input data is very important, and we present a case that Rayleigh testing of time-tagged photons is the most appropriate method to search for quasi-periods. We apply Monte Carlo simulations to extract statistical significances, which we believe are more meaningful than the empirical significances which are often quoted from analysis methods such as Lomb-Scargle. We hope that the work presented here provides a framework for the future examination of jovian X-ray data in the Juno era, where the combination of multiwavelength remote sensing and multi-instrument in situ monitoring will unlock the secrets of the drivers of these dynamic emissions.

We look forward to exploring the conditions under which X-ray quasi-periodicities at Jupiter might be regularly and repeatedly observed, elucidating the drivers of such regular behavior. We also hope that our techniques can be applied to other wavelengths and data sets to build a full picture of the dynamics of Jupiter's auroral zone.

Acknowledgments
C.M.J. is supported by STFC Ernest Rutherford Fellowship ST/L004399/1. D. A. acknowledges support from the Royal Society. We use the IDL scargle.pro code available here: http://www.arm.ac.uk/~csj/idl/PRIMITIVE/scargle.pro. This research has made use of data obtained from the *Chandra Data Archive* and the *Chandra Source Catalogue* and software provided by the *Chandra X-ray Center* (*CXC*) in the application package *CIAO*. C.M.J. acknowledges John Coxon and Peter Boorman for code testing. The authors acknowledge the inputs of both reviewers: their careful and thorough critique has significantly improved the paper and we are grateful for their time.

References

Bélanger, G. (2016). On more sensitive periodogram statistics. *Astophysical Journal*, *822*, 14. https://doi.org/10.3847/0004-637X/822/1/14

Bhardwaj, A., Branduardi-Raymont, G., Elsner, R. F., Gladstone, G. R., Ramsay, G., Rodriguez, P., et al. (2005). Solar control on Jupiter's equatorial X-ray emissions: 26–29 November 2003 XMM-Newton observation. *Geophysical Research Letters*, *32*, L03S08. https://doi.org/10.1029/2004GL021497

Bonfond, B., Grodent, D., Badman, S. V., Gérard, J.-C., & Radioti, A. (2016). Dynamics of the flares in the active polar region of Jupiter. *Geophysical Research Letters*, *43*, 11,963–11,970. https://doi.org/10.1002/2016GL071757

Bonfond, B., Vogt, M. F., Gérard, J.-C., Grodent, D., Radioti, A., & Coumans, V. (2011). Quasi-periodic polar flares at Jupiter: A signature of pulsed dayside reconnections? *Geophysical Research Letters*, *38*, L02104. https://doi.org/10.1029/2010GL045981

Branduardi-Raymont, G., Bhardwaj, A., Elsner, R. F., Gladstone, G. R., Ramsay, G., Rodriguez, P., et al. (2007). A study of Jupiter's aurorae with XMM-Newton. *Astronomy and Astrophysics*, *463*(2), 761–774. https://doi.org/10.1051/0004-6361:20066406

Branduardi-Raymont, G., Elsner, R. F., Galand, M., Grodent, D., Cravens, T. E., Ford, P., et al. (2008). Spectral morphology of the X-ray emission from Jupiter's aurorae. *Journal of Geophysical Research*, *113*, A02202. https://doi.org/10.1029/2007JA012600

Branduardi-Raymont, G., Elsner, R. F., Gladstone, G. R., Ramsay, G., Rodriguez, P., Soria, R., & Waite, J. H. Jr. (2004). First observation of Jupiter by XMM-Newton. *Astronomy and Astrophysics*, *424*, 331–337. https://doi.org/10.1051/0004-6361:20041149

Brazier, K. T. S. (1994). Confidence intervals from the Rayleigh test. *Monthly Notices of the Royal Astronomical Society*, *268*, 709–712. https://doi.org/10.1093/mnras/268.3.709

Buccheri, R., Bennett, K., Bignami, G. F., Bloemen, J. B. G. M., Boriakoff, V., Caraveo, P. A., et al. (1983). Search for pulsed gamma-ray emission from radio pulsars in the COS-B data. *Astronomy and Astrophysics*, *128*, 245–251.

Bunce, E. J., Cowley, S. W. H., & Yeoman, T. K. (2004). Jovian cusp processes: Implications for the polar aurora. *Journal of Geophysical Research*, *109*, A09S13. https://doi.org/10.1029/2003JA010280

Cravens, T. E., Howell, E., Waite, J. H., & Gladstone, G. R. (1995). Auroral oxygen precipitation at Jupiter. *Journal of Geophysical Research*, *100*(A9), 17,153–17,161. https://doi.org/10.1029/95JA00970

Cravens, T. E., & Ozak, N. (2012). Auroral ion precipitation and acceleration at the outer planets. In A. Keiling, et al. (Eds.), *Auroral phenomenology and magnetospheric rrocesses: Earth and other planets* (pp. 287–294). Washington, DC: American Geophysical Union. https://doi.org/10.1029/2011GM001159

Cravens, T. E., Waite, J. H., Gombosi, T. I., Lugaz, N., Gladstone, G. R., Mauk, B. H., & MacDowall, R. J. (2003). Implications of Jovian X-ray emission for magnetosphere-ionosphere coupling. *Journal of Geophysical Research*, *108*(A12), 1465. https://doi.org/10.1029/2003JA010050

DeJager, O. C., Swanepoel, J. W. H., & Raubenheimer, B. C. (1989). A powerful test for weak periodic signals with unknown light curve shape in sparse data. *Astronomy and Astrophysics*, *221*, 180–190.

Dunn, W. R., Branduardi-Raymont, G., Elsner, R. F., Vogt, M. F., Lamy, L., Ford, P. G., et al. (2016). The impact of an ICME on the Jovian X-ray aurora. *Journal of Geophysical Research: Space Physics*, *121*, 2274–2307. https://doi.org/10.1002/2015JA021888

Dunn, W. R., Branduardi-Raymont, G., Ray, L. C., Jackman, C. M., Kraft, R. P., Elsner, R. F., et al. (2017). The independent pulsations of Jupiter's northern and southern X-ray auroras. *Nature Astronomy*, *1*, 758–764. https://doi.org/10.1038/s41550-017-0262-6. [Abbreviated to D17 in this work]

Elsner, R. F., et al. (2005). Simultaneous Chandra X-ray, Hubble Space Telescope ultraviolet, and Ulysses radio observations of Jupiter's aurora. *Journal of Geophysical Research*, *110*, A01207. https://doi.org/10.1029/2004JA010717

Fruscione, A., McDowell, J. C., Allen, G. E., Brickhouse, N. S., Burke, D. J., Davis, J. E., et al. (2006). CIAO: Chandra's data analysis system. In D. R. Silvia & R. E. Doxsey (Eds.), Proceedings of the SPIE (Vol. 6270, pp. 62701V). Retrieved from http://adsabs.harvard.edu/abs/2006SPIE.6270E..1VF

Gibson, A. I., Harrison, A. B., Kirkman, I. W., Lotts, A. P., Macrae, J. H., Orford, K. J., et al. (1982). Transient emission of ultra-high energy pulsed γ rays from Crab pulsar PSR0531. *Nature*, *296*, 1982.

Gladstone, G. R., Waite, J. H. Jr., Grodent, D., Lewis, W. S., Crary, F. J., Elsner, R. F., et al. (2002). A pulsating auroral X-ray hot spot on Jupiter. *Nature*, *415*(6875), 1000–1003. [Abbreviated to G02 in this work]. https://doi.org/10.1038/4151000a

Horne, J. H., & Baliunas, S. L. (1986). A prescription for period analysis of unevenly sampled time series. *Astrophysical Journal: Part I*, *302*, 757–763. https://doi.org/10.1086/164037

Kimura, T., Kraft, R. P., Elsner, R. F., Branduardi-Raymont, G., Gladstone, G. R., Tao, C., et al. (2016). Jupiter's X-ray and EUV auroras monitored by Chandra, XMM-Newton, and Hisaki satellite. *Journal of Geophysical Research: Space Physics*, *121*, 2308–2320. https://doi.org/10.1002/2015JA021893

Leahy, D. A., Elsner, R. F., & Weisskopf, M. C. (1983). On searches for periodic pulsed emission: The Rayleigh test compared to epoch folding. *Astrophysical Journal*, *272*, 256–258. https://doi.org/10.1086/161288

Lomb, N. R. (1976). Least-squares frequency analysis of unequally spaced data. *Astrophysics and Space Science*, *39*, 447–462. https://doi.org/10.1007/BF00648343

MacDowall, R. J., Kaiser, M. L., Desch, M. D., Farrell, W. M., Hess, R. A., & Stone, R. G. (1993). Quasiperiodic Jovian radio bursts: Observations from the Ulysses radio and plasma wave experiment. *Planetary and Space Science*, *41*, 1059–1072. https://doi.org/10.1016/0032-0633(93)90109-F

Mardia, K. V. (1972). *Statistics of directional data*. New York: Academic Press.

Maurellis, A. N., Cravens, T. E., Gladstone, G. R., Waite, J. H., & Acton, L. W. (2000). Jovian X-ray emission from solar X-ray scattering. *Geophysical Research Letters*, *27*(9), 1339–1342. https://doi.org/10.1029/1999GL010723

McKibben, R. B., Simpson, J. A., & Zhang, M. (1993). Impulsive bursts of relativistic electrons discovered during Ulysses' traversal of Jupiter's dusk-side magnetosphere. *Planetary and Space Science*, *41*(11–12), 1041–1058. https://doi.org/10.1016/0032-0633(93)90108-E

Metzger, A. E., Gilman, D. A., Luthey, J. L., Hurley, K. C., Schnopper, H. W., Seward, F. D., & Sullivan, J. D. (1983). The detection of X-rays from Jupiter. *Journal of Geophysical Research*, *88*(A10), 7731–7741. https://doi.org/10.1029/JA088iA10p07731

Nichols, J. D., Yeoman, T. K., Bunce, E. J., Chowdhury, M. N., Cowley, S. W. H., & Robinson, T. R. (2017). Periodic emission within Jupiter's main auroral oval. *Geophysical Research Letters*, *44*, 9192–9198. https://doi.org/10.1002/2017GL074824

Scargle, J. D. (1982). Studies in astronomical time series analysis. II – Statistical aspects of spectral analysis of unevenly spaced data. *The Astrophysical Journal*, *263*, 835. https://doi.org/10.1086/160554

Vaughan, S. (2005). A simple test for periodic signals in red noise. *Astronomy and Astrophysics*, *431*, 391–403. https://doi.org/10.1051/0004-6361:20041453

Vogt, M. F., Bunce, E. J., Kivelson, M. G., Khurana, K. K., Walker, R. J., Radioti, A., et al. (2015). Magnetosphere-ionosphere mapping at Jupiter: Quantifying the effects of using different internal field models. *Journal of Geophysical Research: Space Physics*, *120*, 2584–2599. https://doi.org/10.1002/2014JA020729

Walker, R. J., & Russell, C. T. (1985). Flux transfer events at the Jovian magnetopause. *Journal of Geophysical Research*, *90*, 7397–7404. https://doi.org/10.1029/JA090iA08p07397